

Tunable plasmons in ultrathin metal films

Rinu Abraham Maniyara^{1†}, Daniel Rodrigo^{1†}, Renwen Yu¹, Josep Canet-Ferrer¹, Dhriti Sundar Ghosh¹, Ruchirej Yongsunthon², David E. Baker², Aram Rezikyan², F. Javier García de Abajo^{1,3*}, Valerio Pruneri^{1,3*}

Affiliations:

¹ ICFO- Institut de Ciències Fotòniques, The Barcelona Institute of Science and Technology, 08860 Castelldefels (Barcelona), Spain

² Corning Research and Development Corporation, Sullivan Park, Corning, New York 14831, United States.

³ ICREA- Institució Catalana de Recerca i Estudis Avançats, 08010, Barcelona, Spain.

* Correspondence to: valerio.pruneri@icfo.eu, javier.garciadeabajo@icfo.eu

† Equal contribution

Summary:

The physics of electrons, photons and their plasmonic interactions changes dramatically when one or more dimensions are reduced down to the nanometer scale¹. For example, this principle applies to atomically thin graphene, which exhibits unique electrical transport and optical properties, such as very high mobility and long-lived highly confined plasmon waves, with the unparalleled ability of being dynamically tunable through electrostatic gating or chemical doping^{2,3}. These properties have been extensively exploited with great potential for a wide range of applications, including optical modulation and sensing^{4,5}. Similarly, ultrathin metal films (UTMFs) down to atomic thickness have been shown to possess new quantum optical effects^{6,7}, peculiar dielectric properties⁸, and are theoretically predicted to lead to strong plasmons with potential use for light modulation^{9,10}. However, truly two-dimensional plasmonics in metals has so far been elusive due to difficulty in producing large areas of sufficiently thin continuous UTMFs. Thanks to a novel deposition technique that allows percolation even at 1 nm thickness, we demonstrate plasmons in few-nanometer gold UTMFs, with clear evidence of new dispersion regimes and large electrical tunability, that are not possible in thicker metals. With proper patterning, we show plasmon resonances from near-(1.5 μ m) to mid-infrared (5 μ m) wavelengths in different thickness UTMFs, with evident dispersion bending and deviation from the light line for the thinner (3 nm) films. Correspondingly, we achieve reversible wavelength shifts for the plasmonic resonances of about 200 nm and 700 nm at around 2 and 4.5 μ m, respectively, together with transmission modulations up to 30%, by applying an electrical gating voltage of ± 2 V through ion gel. The demonstrated two-dimensional behavior together with large electro-optic tunability open a new path for metals in plasmonic applications, such as electro-optic modulation, bio-sensing, and smart windows.

Main text:

Since ancient times, plasmons in noble metals such as silver and gold have been used to color glass, while the last two decades have witnessed an explosion in the number of applications of these excitations triggered by an improved understanding of their origin and behavior, as well as by the availability of more sophisticated means to synthesize and pattern the metals¹¹⁻¹⁶. Here we show that, similarly to graphene¹⁷, ultrathin metal films (UTMFs) with a sufficiently low nanometric thickness can support two-dimensional plasmons. In particular, we achieve new dispersion regimes and large optical tunability by electrical gating. These experiments are made possible thanks to a novel deposition technique in which copper is used as a seed layer to produce large areas of gold UTMFs. The technique (physical vapor deposition) avoids the problem of island-like growth of unseeded gold at small thickness, giving rise to percolated films, and has the crucial advantage of being industrially scalable. We remark that in this work electrical percolation is observed down to a nominal (mass-equivalent) thickness t of 1 nm, while plasmonic behavior is observed for $t=3$ nm. t is determined by the deposition rate and may differ from the geometrical thickness. However, for samples with nominal gold thickness equal and above 3 nm real (geometrical) values measured with atomic-force microscopy (AFM) are relatively close to the nominal values.

Direct evaporation of gold on substrates such as glass and other inorganic materials (e.g., CaF₂) causes the gold UTMF to grow in metallic islands of irregular shape (Volmer-Weber growth mode) during the initial growth stages due to the poor wetting of gold^{18,19} (Fig. 1a). The key idea introduced in our UTMFs fabrication is the use of a sputtered copper seed layer with $t \sim 1$ nm, that was already shown producing lower percolation threshold in silver films²⁰. In this work, the copper seed layer undergoes oxidation prior to the gold evaporation. The resulting percolated and polycrystalline gold UTMF is shown in Fig. 1b. For a nominal thickness $t=3$ nm determined by extrapolation of the deposition rate, in turn calibrated by a quartz crystal microbalance, we find a roughness $R_q = 0.22$ nm measured with atomic-force microscopy (AFM) at 3 nm lateral resolution (Fig. 1 a,b). Long-range continuity of the seeded gold film is observed in scanning electron microscope (SEM) images at 3 nm resolution, in contrast to the disconnected geometry observed in unseeded films. We measured a geometrical (real) thickness of 4.42 ± 0.14 nm using AFM for deposition of a mass-equivalent thickness $t=3$ nm of gold seeded by 1 nm of copper on a 285 nm thick native silica oxide on silicon substrate. The AFM thickness value is also consistent with scanning transmission electron microscopy (STEM) images with sub-angstrom resolution, which additionally confirm good continuity of the film. The fact that the geometrical thickness is slightly larger than the total mass-equivalent thickness (4 nm) could be due to the formation of copper oxide with a volume larger than the original metal.

In order to characterize the long-range connectivity and the percolation thickness of gold UTMFs, we measure visible and near infrared transmission spectra for different t (Fig. 1c). The unseeded gold UTMFs present a transmission dip at approximately $\lambda=600-650$ nm for low coverage, which we attribute to localized optical modes as a signature of the presence of electrically isolated metallic islands^{21,22}. The film percolates (i.e., the gold becomes physically connected) for $t \geq 7$ nm, as is evidenced by the disappearance of the noted resonance and the progressively lower transmission at longer infrared wavelengths. The measured spectra for the Cu-seeded gold UTMFs (Fig. 1d) become noticeably different from the unseeded films at low

coverage, in which the transmission decreases at longer wavelengths, exhibiting a typical behavior of continuous metals down to $t=1$ nm, and therefore indicating an unprecedentedly low percolation depth.

In addition to the optical measurements, we study the electrical properties of the deposited UTMFs (Fig. 1e). The minimum nominal (mass-equivalent) gold thickness for which a UTMF is electrically conductive is $t=1$ nm and $t=7$ nm for seeded and unseeded growth, respectively, in good agreement with the optical results. For $t=1$ nm, the seeded UTMF has a sheet resistance of ~ 1.5 $\text{k}\Omega/\square$, which is comparable to single layer graphene, while for $t=3$ nm it substantially decreases to $74 \Omega/\square$. We also observe that for $t \geq 3$ nm, the electrical scattering time τ of the seeded gold UTMFs is in all cases in between 3 and 10 times smaller than in bulk metal.

We study next the infrared plasmonic properties of seeded gold UTMFs with t down to 3 nm. To this end, we pattern them into nanoribbon structures of width W and period P , which enable an efficient excitation of plasmonic modes by illumination with normally-incident infrared light (Fig. 2a). The nanostructuring of gold UTMFs on infrared transparent CaF_2 substrates is carried out with electron beam lithography and argon reactive ion etching (Fig. 2b). The resulting transmittance and reflectance spectra are shown in Fig. 2c for $t=3$ nm, exhibiting strong resonances at near- and mid-infrared wavelengths. Such resonance peaks reveal that, despite the ultrathin nature of the film, the level of optical damping is sufficiently low to support plasmonic modes. By comparison with electromagnetic simulations, we extract an effective optical damping rate $\Gamma=0.19$ eV in our seeded 3 nm gold UTMFs, which is approximately 3 times larger than in bulk metal²³, whereas in previous thin films one needs to add a Lorentz component to the permittivity to account for extra damping²⁴. We remark that the plasmonic response of thin films are rather independent of their detailed nanoscale morphology in the current regime of deep-subwavelength thickness (i.e., porous films with a geometrical thickness up to a factor of two higher than the mass-equivalent thickness t would result in the same plasmon dispersion within the accuracy of the present study).

To further understand the nature of these plasmonic modes we have measured the spectral response of nano-patterned seeded gold UTMFs with mass-equivalent thicknesses $t=6$ nm and 15 nm (Fig. 2d). We observe that for these larger thicknesses the plasmonic resonance shifts toward shorter wavelengths. This is a well-known plasmonic effect, typical of metals in the visible wavelength range. The behavior becomes clearer by mapping the ribbons resonance obtained from experiments into a dispersion diagram (Fig. 2e). For large thickness ($t=15$ nm) the ribbon dispersion follows closely the light line dispersion (accounting for the surrounding refractive index). However, as the metal layer becomes thinner ($t=3$ nm) there is a clear dispersion bending and a deviation from the light line, which is also predicted by the theoretical loss function that evaluates plasmonic energy dissipation (Fig. 2f). The bending observed in the dispersion diagram reveals the plasmonic nature of the infrared resonances modes in UTMFs when the thickness becomes sufficiently small. Importantly, the dispersion bending takes place at metal thicknesses for which the UTMF becomes infrared transparent (see inset in Fig. 2f), indicating that the plasmonic effects arise when the UTMF is thinner than the penetration depth of the infrared field. The physical origin of the measured plasmonic response lies in the low surface carrier density of UTMF when the mass-equivalent thickness t becomes sufficiently small.

Next, we explore the electrical gating of plasmons in UTMFs. As illustrated in Fig. 3a, the seeded gold UTMF ribbons are spin coated with an ion gel composed of EMIM-TFSI and PS-PEO-PS polymer (see Methods) and an electrostatic voltage (V_g) is applied between the ribbons and an external top electrode. We show in Fig. 3b (experiments) and Fig. 3c (theory) infrared

spectra of selected ribbon arrays with mass-equivalent thickness t of 3 nm, 6 nm, and 15 nm for different gate voltages from $V_g = +2$ V to -2 V. We observe in the experiments that the plasmonic resonance remains constant for $t=15$ nm, it can be slightly modulated for $t=6$ nm, and it is highly tunable for $t=3$ nm. The corresponding experimental wavelength shift is plotted in Fig. 3C and reaches $\Delta\lambda=200$ nm for $t=3$ nm and a smaller value of $\Delta\lambda=50$ nm for 6 nm, whereas for $t=15$ nm it is below the precision of experiment. These changes are reversible with voltage and, in some cases, present a residual hysteresis. The wavelength shift is a clear evidence of a substantial change in the surface carrier density as a result of voltage gating. As expected, for negative gating voltages there is a decrease in density of conduction electrons, which in turn produces a redshift of the plasmonic resonance. From our infrared simulations (Fig. 3d) we observe that the wavelength shifts can be explained by an effective surface carrier density variation up to $\Delta n_s=3\times 10^{15}$ carriers/cm², which corresponds to the number of carriers associated with a change of mass-equivalent thickness $\Delta t=0.5$ nm in the gold layer and is consistent with the modulation observed in electrical transport experiments by independent groups^{25,26}. For this surface carrier density modulation, the relative variation of carrier density is 17%, 8%, and 3% in films of $t=3$ nm, 6 nm, and 15 nm, respectively, which explains the widening of the wavelength tuning range for lower UTMF thicknesses.

In addition to the wavelength shift, there is also a very significant modulation of the optical transmission, especially for $t=3$ nm, in which the resonance peak amplitude can be tuned from 39% to 55% transmittance. This large modulation cannot be explained by a carrier density change alone. Indeed, simulations indicate that for $t=3$ nm, the carrier density variation is responsible for less than one fourth of the transmission modulation range. Instead, the additional mechanism dominating amplitude modulation could be associated with changes in carrier mobility, and consequently optical damping, affecting the amplitude and width of the plasmonic peak. Our simulations show good agreement with experiment when the Drude damping Γ for $t=3$ nm is changed from 0.19 eV to 0.32 eV when varying the voltage V_g from +1.5 V to -2.0 V, while for $t=6$ nm it needs to be changed from 0.10 eV to 0.14 eV. The fact that the largest damping modulation takes places for the thinnest UTMFs indicates that surface scattering may be the dominant damping channel at such small thicknesses.

We explore also the tunability of UTMFs at different wavelengths by adjusting the ribbon width W . In Fig. 3e we show the transmission amplitude and resonance wavelength of the plasmonic peak for varying voltage V_g , ribbon width W , and mass-equivalent metal thickness t . For the thinnest UTMF under consideration ($t=3$ nm) we detect tunable plasmons in the near-IR ($\lambda=1.5$ μ m) and in the mid-IR ($\lambda=5$ μ m) for the narrowest ($W=150$ nm) and widest ($W=800$ nm) ribbons, respectively. The transmission and wavelength tuning ranges progressively decrease as the UTMF becomes thicker. The average transmission modulation (ΔT) is 14.4%, 3.0%, and <1% for $t=3$ nm, 6 nm, and 15 nm, respectively. An analogous trend is found in the average wavelength tuning range ($\Delta\lambda/\lambda_0$), which is 13.6%, 2.1%, and <1% for $t=3$ nm, 6 nm, and 15 nm, respectively.

Our results demonstrate plasmons in ultrathin gold films, extending the plasmonic regime to infrared wavelengths and providing a broad dynamically tunable optical response. These characteristics, combined with a large-scale fabrication approach, can find applications in transparent conductors, plasmon-enhanced spectroscopy, optical biosensing, and electrochromic devices.

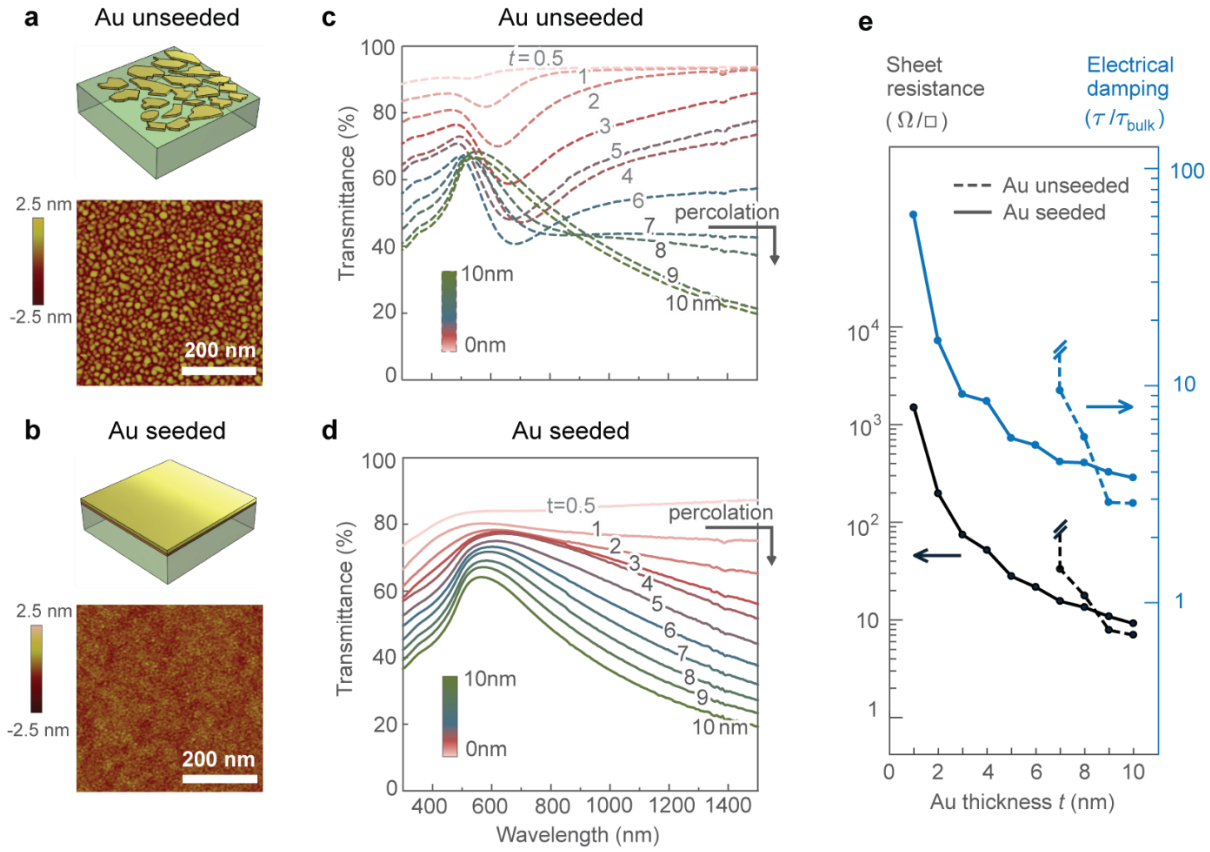


Fig. 1. Ultrathin metal films. **a, b**, Conceptual view and atomic force microscope images of gold ultrathin metal films (UTMFs) of mass-equivalent thickness $t \approx 3$ nm grown on 285 nm thick native silica oxide on Silicon substrates without and with a copper seed layer. Unseeded gold grows with discontinuous island-like morphology, while seeded gold produces continuous and relatively smooth films. **c,d**, Near-infrared and visible transmission spectrum of unseeded and seeded UTMFs grown on fused silica for different gold thicknesses t . The spectra of unseeded gold UTMFs **c**, show transmission dips at around 600 nm for t below 7 nm, corresponding to localized plasmon resonances of isolated gold islands and revealing an optically disconnected layer. In contrast, the spectra of seeded gold UTMFs **d**, show progressively decreasing transmission at near-infrared wavelengths for t above 1 nm, demonstrating long-range connectivity. **e**, Electrical sheet resistance and damping of seeded and unseeded gold UTMFs as a function of film thickness t . Unseeded gold UTMFs are only conductive for $t \geq 7$ nm (percolation thickness), while seeded UTMFs are conductive even down to $t = 1$ nm.

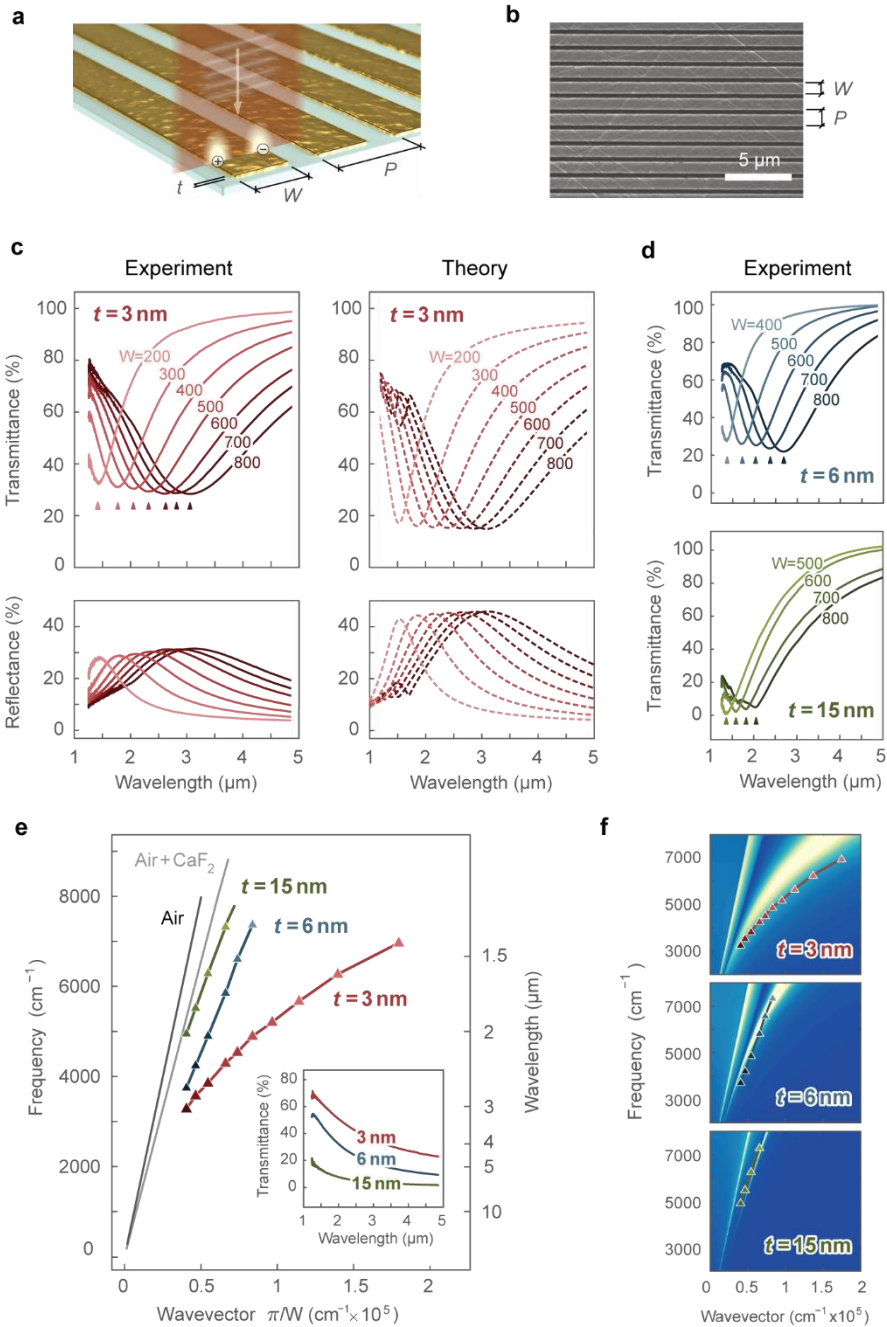


Fig. 2. Infrared plasmons in ultrathin metal films. **a**, Conceptual view and **b**, scanning electron microscope of UTMF seeded gold nanoribbons of width W , period P , and mass-equivalent thickness t , fabricated on CaF_2 substrates. **c**, Measured and simulated spectra of UTMF nanoribbons showing plasmonic resonances from near-to mid-infrared for different ribbon widths W and fixed thickness $t=3$ nm. We use a gold Drude model with damping $\Gamma=0.19$ eV in the simulations. **d**, Measured transmission spectra of UTMF nanoribbons for $t=6$ nm and $t=15$ nm. **e**, Experimental dispersion curves of UTMF plasmons for different thicknesses obtained from the ribbon width and resonance wavelength. The thickest ribbons ($t=15$ nm) approach a light-line dispersion (solid grey lines), while the thinnest ribbons ($t=3$ nm) show a dispersion bending characteristic of plasmonic modes. Inset: Measured transmittance spectra of continuous seeded gold UTMFs for different thicknesses. **f**, Comparison between experimental dispersion curves of UTMF plasmons and the theoretical loss function for different thicknesses. The gold Drude damping factors used in the calculations are $\Gamma=0.19$ eV, 0.10 eV, and 0.07 eV for $t=3$ nm, 6 nm, and 15 nm, respectively, as obtained by fitting the experimental full width at half maximum in the plasmon spectral features.

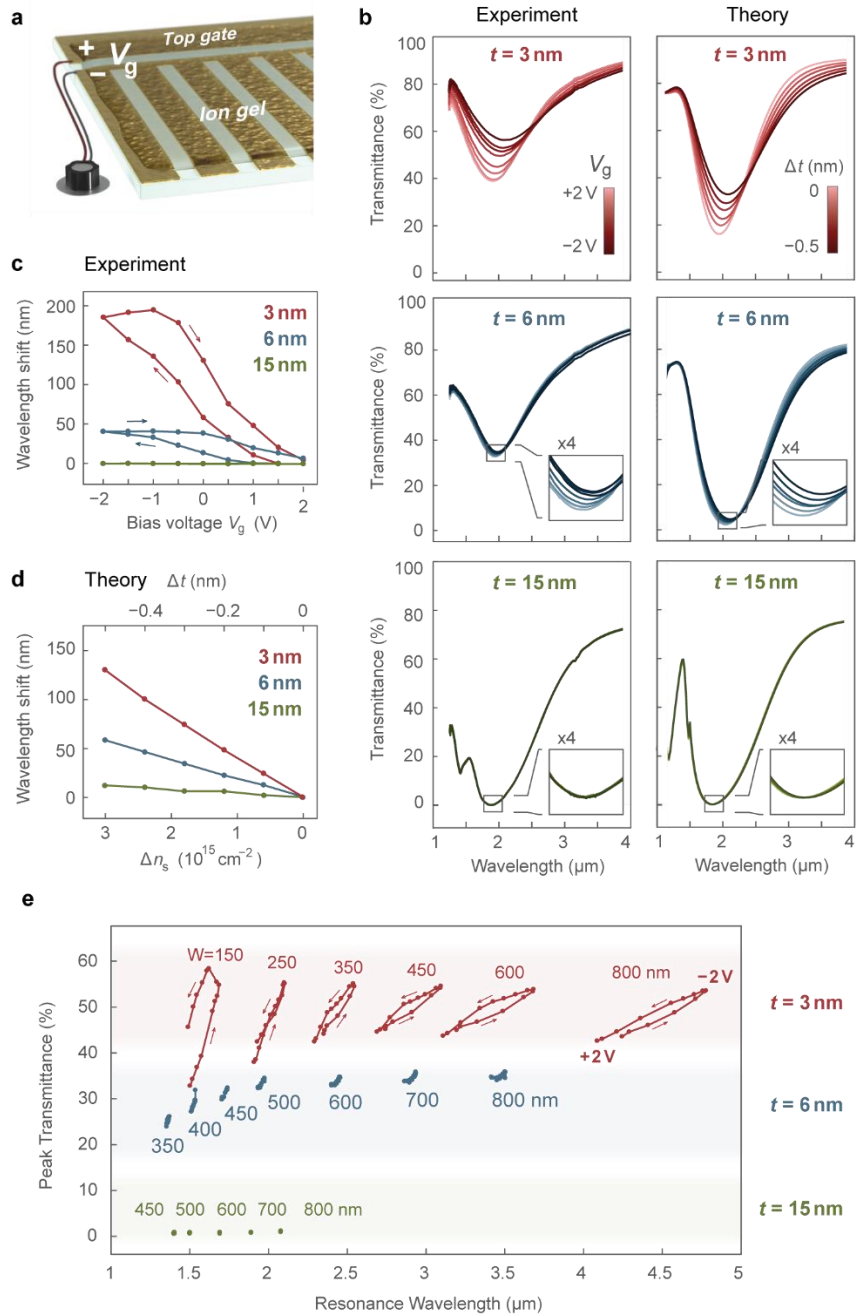


Fig. 3. Tunable plasmons in ultrathin metal films. **a**, Conceptual view of the dynamic tuning of UTMF nanoribbons by ion-gel gating. **b**, Measured and simulated transmission spectra of tunable nanoribbons resonating at $\lambda=2\text{ }\mu\text{m}$ for thicknesses $t=3\text{ nm}$, 6 nm , and 15 nm and widths $W=250\text{ nm}$, 500 nm , and 700 nm , respectively. The experimental spectra correspond in all cases to gating voltages V_g from $+2\text{ V}$ (light color) to -2.0 V (dark color). The theoretical spectra correspond to nanoribbons with an effective thickness $t_{\text{eff}}=t+\Delta t$, using an effective thickness modulation between $\Delta t=0$ (light color) and $\Delta t=0.5\text{ nm}$ (dark color). The optical damping factors Γ for gold used in the simulations vary from 0.19 eV to 0.32 eV for $t=3\text{ nm}$, from 0.10 to 0.14 eV for $t=6\text{ nm}$, and fixed at 0.07 eV for $t=15\text{ nm}$. **c**, Measured shift of the plasmonic resonance wavelength over a full voltage cycle for different gold seeded UTMF thicknesses t . **d**, Simulated shift of the plasmonic resonance wavelength for different mass-equivalent thicknesses t , obtained by varying the effective optical thickness Δt , or equivalently, the effective surface carrier density Δn_s . **e**, Measured resonance wavelength and transmission amplitude of the plasmonic peak for different thicknesses t , ribbon widths W , and gating voltages V_g in the $+2\text{ V}$ to -2 V range.

References and Notes:

1. Britnell, L. *et al.* Strong light-matter interactions in heterostructures of atomically thin films. *Science* **340**, 1311–1314 (2013).
2. Geim, A. K. & Novoselov, K. S. The rise of graphene. *Nat. Mater.* **6**, 183–191 (2007).
3. Koppens, F. H. L., Chang, D. E. & García De Abajo, F. J. Graphene plasmonics: A platform for strong light-matter interactions. *Nano Lett.* **11**, 3370–3377 (2011).
4. Liu, M. *et al.* A graphene-based broadband optical modulator. *Nature* **474**, 64–67 (2011).
5. Rodrigo, D. *et al.* Mid-infrared plasmonic biosensing with graphene. *Science* **349**, 165–168 (2015).
6. Qian, H., Xiao, Y. & Liu, Z. Giant Kerr response of ultrathin gold films from quantum size effect. *Nat. Commun.* **7**, 13153 (2016).
7. Dryzek, J. & Czapla, A. Quantum size effect in optical spectra of thin metallic films. *Phys. Rev. Lett.* **58**, 721–724 (1987).
8. Hövel, M., Gompf, B. & Dressel, M. Dielectric properties of ultrathin metal films around the percolation threshold. *Phys. Rev. B - Condens. Matter Mater. Phys.* **81**, 035402 (2010).
9. Manjavacas, A. & García de Abajo, F. J. Tunable plasmons in atomically thin gold nanodisks. *Nat. Commun.* **5**, 3548 (2014).
10. García De Abajo, F. J. & Manjavacas, A. Plasmonics in atomically thin materials. *Faraday Discuss.* **178**, 87–107 (2015).
11. Stockman, M. I. Nanoplasmonics: past, present, and glimpse into future. *Opt. Express* **19**, 22029–22106 (2011).
12. Tame, M. S. *et al.* Quantum plasmonics. *Nat. Phys.* **9**, 329 (2013).
13. Lu, Y., Huang, J. Y., Wang, C., Sun, S. & Lou, J. Cold welding of ultrathin gold nanowires. *Nat. Nanotechnol.* **5**, 218–224 (2010).
14. Fang, N., Lee, H., Sun, C. & Zhang, X. Sub-diffraction-limited optical imaging with a silver superlens. *Science* **308**, 534–537 (2005).
15. Nagpal, P., Lindquist, N. C., Oh, S. H. & Norris, D. J. Ultrasmooth patterned metals for plasmonics and metamaterials. *Science* **325**, 594–597 (2009).
16. Brown, A. M., Sheldon, M. T. & Atwater, H. A. Electrochemical tuning of the dielectric function of Au nanoparticles. *ACS Photonics* **2**, 459–464 (2015).
17. Grigorenko, A. N., Polini, M. & Novoselov, K. S. Graphene plasmonics. *Nat. Photonics* **6**, 749–758 (2012).
18. Vogt, K. W., Kohl, P. A., Carter, W. B., Bell, R. A. & Bottomley, L. A. Characterization of thin titanium oxide adhesion layers on gold: resistivity, morphology, and composition. *Surf. Sci.* **301**, 203–213 (1994).
19. Dalacu, D. & Martinu, L. Optical properties of discontinuous gold films: finite-size effects. *J. Opt. Soc. Am. B-Optical Phys.* **18**, 85–92 (2001).
20. Formica, N. *et al.* Ultrastable and atomically smooth ultrathin silver films grown on a

copper seed layer. *ACS Appl. Mater. Interfaces* **5**, 3048–3053 (2013).

- 21. Jarrett, D. N. & Ward, L. Optical properties of discontinuous gold films. *J. Phys. D. Appl. Phys.* **9**, 10 (1976).
- 22. Kreibig, U. & Vollmer, M. *Optical Properties of Metal Clusters*. Springer (1995).
- 23. Johnson, P. B. & Christy, R. W. Optical constants of the noble metals. *Phys. Rev. B* **6**, 4370 (1972).
- 24. Brandt, T., Hövel, M., Gompf, B. & Dressel, M. Temperature- and frequency-dependent optical properties of ultrathin Au films. *Phys. Rev. B - Condens. Matter Mater. Phys.* **78**, 205409 (2008).
- 25. Daghero, D. *et al.* Large conductance modulation of gold thin films by huge charge injection via electrochemical gating. *Phys. Rev. Lett.* **108**, 066807 (2012).
- 26. Petach, T. A., Lee, M., Davis, R. C., Mehta, A. & Goldhaber-Gordon, D. Mechanism for the large conductance modulation in electrolyte-gated thin gold films. *Phys. Rev. B - Condens. Matter Mater. Phys.* **90**, 081108 (2014).

Acknowledgments: We acknowledge Kavitha Kalavoor, Miriam Marchena and Johann Osmond for their help in the experiments and fruitful discussions. **Funding:** We acknowledge financial support from the Spanish Ministry of Economy and Competitiveness through the “Severo Ochoa” programme for Centers of Excellence in R&D (SEV-2015-0522), OPTO-SCREEN (TEC2016-75080-R), and Grant No. MAT2017-88492-R, from Fundació Privada Cellex, from Generalitat de Catalunya through the CERCA program, and AGAUR 2017 SGR 1634, and from the European Union Seventh Framework Programme under grant agreement no. 609416 ICFONest. J. C.-F. also thanks MINECO for his research grant funded by means of the program Juan de la Cierva (Grant No. FPD-2013-18078).

Author contributions: V.P. conceived the experiments and with the help of R.A.M and D.R designed them. R.A.M and D.R with the help of J.C.-F, D.S.G, R.Y, D.E.B and R.A. carried out the experiments and characterizations. D.R and R.Y performed all the optical simulations and calculations. D.R, V.P, F.J.G.A, and R.A.M wrote the manuscript. All authors contributed to the interpretation of the results and manuscript writing. F.J.G.A. and V.P. proposed the research project.